

Numerical Study of Polymer Composites in Contact

L. Rodríguez-Tembleque¹, A. Sáez¹ and F.C. Buroni¹

Abstract: A boundary element based formulation is applied to study numerically the tribological behavior of fiber-reinforced plastics (FRP) under different frictional contact conditions, taking into account the micromechanics of FRP. Micromechanical models presented consider continuous and short fiber reinforced plastics configurations. The Boundary Element Method (BEM) with an explicit approach for fundamental solutions evaluation is considered for computing the elastic influence coefficients. Signorini's contact conditions and an orthotropic law of friction on the potential contact zone are enforced by contact operators over the augmented Lagrangian. The proposed methodology is applied to study carbon FRP under frictional contact. The obtained numerical results illustrate how the fiber orientation, fiber volume fraction, fiber length and sliding orientation affect the normal and tangential contact compliance, as well as the contact traction distribution.

Keywords: Fiber Reinforced Plastics, Composite Materials, Anisotropic Friction, Contact Mechanics, Boundary Element Method.

1 Introduction

Fiber-reinforced composite materials are being used increasingly for numerous applications in many different structural and mechanical components (i.e. in biomedical purposes like modern orthopaedic medicine and prosthetic devices [Scholz, Blanchfield, Bloom, Coburn, Elkington, Fuller, Gilbert, Muflahi, Pernice, Rae, Trevarthen, White, Weaver, and Bond (2011)]). Although the fiber-reinforced plastics (FRP) are widely applied, much of the knowledge on their tribological behavior is empirical. A study of their tribological response has not been fully completed, especially in the numerical area, where there are not many numerical formulations that allow to analyze these polymer composites under different frictional contact conditions, taking into account the tribological characteristics of these materials.

¹ Escuela Técnica Superior de Ingeniería, Universidad de Sevilla, Camino de los Descubrimientos s/n, Sevilla E-41092, Spain. (email: luisroteso@us.es)

Some experimental works have studied the significant influence of fiber orientation on the wear and frictional behavior of FRP composites. It has to be mentioned the works of [Ohmae, Kobayashi, and Tsukizoe (1974)], [Sung and Suh (1979)], [Tsukizoe and Ohmae (1983)], [Cirino, Friedrich, and Pipes (1988)], [Jacobs, Friedrich, Marom, Schulte, and Wagner (1990)], [Vishwanath, Verma, and Rao (1993)], and more recently, [Larsen, Andersen, Thorning, Horsewell, and Vigild (2007)]. These experimental works showed that the coefficient of friction depends on several factors including the combination of materials, the surface roughness or the fiber orientation (i.e. the largest coefficient of friction was obtained when the sliding was normal to the fiber orientation, while the lowest one was obtained when the fiber orientation was transverse). Even considering a sliding direction on a plane parallel to the direction of fibers, [Ohmae, Kobayashi, and Tsukizoe (1974)] observed that the coefficient of friction sliding in parallel direction was smaller than in the transverse direction. In summary, there is experimental evidence that it is not only important to consider anisotropy of the bulk material properties but also the anisotropy of the surface properties.

The theoretical studies on anisotropic elastic contact were initially treated by [Willis (1996)], who provided an analytical treatment for contact of two non-conforming bodies, and later by [Turner (1980)], who considered the special case of transversely isotropic solids in contact such that their axes of symmetry are both parallel to the common normal at the point of contact. Willis' analysis was particularized to a transversely isotropic medium by [Gladwell (1980)]. More recently it should be mentioned the analytical works of [Vlassak and Nix (1993, 1994)] [Vlassak, Ciavarella, Barber, and Wang (2003)], [Hwu and Fan (1998)], [Swadener and Pharr (2001)], and [Batra and Jiang (2008)], [Jiang and Batra (2010)], [Ning and Lovell (2002)], [Ning, Lovell, and Morrow (2004)], [Ning, Lovell, and Slaughter (2006)] or [Bagault, Nélias, and Baietto (2012)] and [Bagault, Nélias, Baietto, and Ovaert (2013)]. However due to their intrinsic mathematical complexity, analytical solutions incorporate several restrictive assumptions, e.g. rigid indenter, half-plane space, etc.

In the numerical context, some works based on the Finite Element Method (FEM) studied some particular contact problem between composites: it has to be mentioned the works of [Xiaoyu (1995)] and [Lovell (1998)]. The indentation problem of fiber reinforced polymer was initially studied by [Vàradi, K., Flöck, and Friedrich (1998)], who later presented in [Vàradi, Nèder, Friedrich, and Flöck (1999)] a FEM formulation involving macro- and micro-contact analysis, and more recently, [Goda, Vàradi, Wetzel, and Friedrich (2004a,b)] studied the fiber-matrix debonding process. As it can be observed in these works, it is necessary a very fine mesh to approximate the contact problem between the anisotropic solids.

Alternatively, the Boundary Element Method (BEM) [Aliabadi (2002)] and [Breb-
bia and Dominguez (1992)] has been shown very suitable to study contact prob-
lems: [Mantic, Graciani, París, and Varna (2005)], [Graciani, Mantic, París, and
Varna (2009)], [Abascal and Rodríguez-Tembleque (2007)], [Rodríguez-Tembleque
and Abascal (2010a,b, 2013)], [Rodríguez-Tembleque, Buroni, Abascal, and Sáez
(2011)], and [Rodríguez-Tembleque, Abascal, and Aliabadi (2010, 2011, 2012a,b)],
since the contact problem is essentially a boundary problem.

This work presents a boundary element formulation to study fiber-reinforced ma-
terials under different frictional contact conditions, whose main feature is that the
methodology allows to analyze these polymer composites taking into account both
the mechanical and the tribological anisotropic characteristics (i.e. anisotropic
bulk properties and orthotropic frictional conditions). Furthermore, the formulat-
ion considers micromechanical models for continuous FRP ([Hopkins and Chamis
(1988)]) and short FRP ([Halpin and Kardos (1976)]) that also makes it possible
to consider the influence of fiber volume fraction and fiber length. The BEM, with
an explicit approach for fundamental solutions evaluation [Buroni, Ortiz, and Sáez
(2011)], is implemented to compute the elastic influence coefficients. The contact
methodology considered in this work is based on the augmented Lagrangian form-
ulation works of [Alart and Curnier (1991)], [Klarbring (1992, 1993)], [Wrig-
gers (2002)] and [Laursen (2002)], but adapted for an orthotropic friction law
[Rodríguez-Tembleque, Abascal, and Aliabadi (2012a,b)] and [Rodríguez- Tem-
bleque and Abascal (2013)]. The methodology and the proposed algorithm are
illustrated with some examples, in which different studies on FRPs are presented.
In these numerical examples, the influence of fiber volume fraction, fiber length,
fiber orientation and sliding orientation on contact variables is clearly observed and
discussed in detail.

2 Boundary integral equations

2.1 Explicit boundary element equations

Consider a linear anisotropic elastic body Ω , with boundary $\partial\Omega$ defined in a Carte-
sian coordinate system $\{x_i\}$ ($i = 1 - 3$) in \mathbb{R}^3 . The general anisotropic behavior is
characterized by a fourth-rank elasticity tensor with components C_{ijkl} , verifying
the symmetry relations $C_{ijkl} = C_{jikl}$, $C_{ijkl} = C_{ijlk}$ and $C_{ijkl} = C_{klij}$. The BEM
formulation is well known and can be found in many classical texts such as [Breb-
bia and Dominguez (1992)] and [Aliabadi (2002)]. For a boundary point ($P \in \partial\Omega$),
the *Somigliana identity* can be written as:

$$\tilde{\mathbf{C}} \mathbf{u}(P) + CPV \left\{ \int_{\partial\Omega} \mathbf{T}^* \mathbf{u} dS \right\} = \int_{\Omega} \mathbf{U}^* \mathbf{b} d\Omega + \int_{\partial\Omega} \mathbf{U}^* \mathbf{t} dS \quad (1)$$

where \mathbf{u} , \mathbf{t} and \mathbf{b} are, respectively, the displacements, the boundary tractions and the body forces of Ω . $\mathbf{U}^* = \{U_{ij}^*(P, Q)\}$ is the fundamental solution tensor for displacement (free-space Green's functions), and $\mathbf{T}^* = \{T_{ij}^*(P, Q)\}$ stands for the tractions fundamental solution at point Q in the i th direction due to a unit load applied at point P in the j th direction. The matrix $\tilde{\mathbf{C}}$ is equal to $\frac{1}{2} \mathbf{I}$ for a smooth boundary $\partial\Omega$, and $CPV \{ \int \cdot dS \}$ denotes the *Cauchy Principal Value* of the integral $\int \cdot dS$.

The displacement fundamental solution for anisotropic media can be expressed as a singular term by a regular modulation function \mathbf{H} as

$$\mathbf{U}^*(r\hat{\mathbf{e}}) = \frac{1}{4\pi r} \mathbf{H}(\hat{\mathbf{e}}) \tag{2}$$

where $r = \|\mathbf{x}(Q) - \mathbf{x}(P)\|$ and $\hat{\mathbf{e}} = (\mathbf{x}(Q) - \mathbf{x}(P))/r$, being $\|\cdot\|$ the *Euclidian norm*. $\mathbf{H}(\hat{\mathbf{e}})$ is one of the three Barnett-Lothe tensors which is symmetric and positive-definite. The tensor $\mathbf{H}(\hat{\mathbf{e}})$ can be evaluated as Ting and Lee (1997)

$$\mathbf{H}(\hat{\mathbf{e}}) = \frac{1}{\pi} \int_{-\infty}^{+\infty} \Gamma^{-1}(p) dp \tag{3}$$

with $\Gamma(p) = \mathbf{Q} + (\mathbf{R} + \mathbf{R}^T)p + \mathbf{T}p^2$, expressed in terms of the parameter p , and

$$Q_{jk} = C_{ijkl}\hat{n}_i\hat{n}_l \quad R_{jk} = C_{ijkl}\hat{n}_i\hat{m}_l \quad T_{jk} = C_{ijkl}\hat{m}_i\hat{m}_l \tag{4}$$

where \hat{n}_i and \hat{m}_i are the components of any two mutually orthogonal unit vectors such that $\{\hat{\mathbf{n}}, \hat{\mathbf{m}}, \hat{\mathbf{e}}\}$ is a right-handed triad. Repeated index implies sum.

The components of the traction fundamental solution follow easily from the derivative of the displacement fundamental solution and further substitution into Hook's law as

$$T_{ik}^* = C_{ijlm}\eta_j \frac{\partial U_{lk}^*}{\partial x_m} \tag{5}$$

where η_j are the components of the external unit normal vector to the boundary $\partial\Omega$ at point Q . The derivative of the Green's function may be expressed in a similar way to equation (2), as a singular term by a modulation function which only depends on $\hat{\mathbf{e}}$ as

$$\frac{\partial \mathbf{U}^*(r\hat{\mathbf{e}})}{\partial x_q} = \frac{1}{4\pi r^2} \frac{\partial \tilde{\mathbf{U}}^*(\hat{\mathbf{e}})}{\partial x_q} \tag{6}$$

where, according to [Lee (2003)], the components of the modulation function are given by

$$\frac{\partial \tilde{U}_{ij}^*(\hat{\mathbf{e}})}{\partial x_l} = -\hat{e}_l H_{ij} + \frac{C_{pqrs}}{\pi} (M_{lqiprj}\hat{e}_s + M_{sliprj}\hat{e}_q) \tag{7}$$

The M_{sliprj} integrals (7) have the following representation in terms of the parameter p [Lee (2003)]:

$$M_{ijklmn} = \frac{1}{|\mathbf{T}|^2} \int_{-\infty}^{+\infty} \frac{\Phi_{ijklmn}(p)}{(p-p_1)^2(p-p_2)^2(p-p_3)^2} dp \quad (8)$$

where \mathbf{T} has been previously defined in (4), p_α are the Stroh's eigenvalues and corresponds to the three complex roots of the sixth-order polynomial equation $|\Gamma(p)| = 0$ with positive imaginary part Ting (1996). In equation (8),

$$\Phi_{ijklmn}(p) := \frac{B_{ij}(p)\hat{\Gamma}_{kl}(p)\hat{\Gamma}_{mn}(p)}{(p-\bar{p}_1)^2(p-\bar{p}_2)^2(p-\bar{p}_3)^2} \quad (9)$$

has been introduced together with the definition of $B_{ij} := \hat{n}_i\hat{n}_j + (\hat{n}_i\hat{m}_j + \hat{m}_i\hat{n}_j)p + \hat{m}_i\hat{m}_j p^2$, being $\hat{\Gamma}_{jk}$ the adjoint of Γ_{jk} , defined as $\Gamma_{pj}\hat{\Gamma}_{jk} = |\Gamma(p)|\delta_{pk}$, where δ_{pk} is the Kronecker delta.

In order to provide an explicit boundary element formulation, the Cauchy's residue theory for multiple poles is applied to evaluate the integrals in (3) and (8), so no integration is performed. In addition, possible repeated Stroh's eigenvalues are allowed in this formulation (see [Buroni, Ortiz, and Sáez (2011)] for details). Recently, [Buroni and Sáez (2013)] have derived new unique and explicit expressions for the anisotropic fundamental solutions that may be used as an alternative evaluation scheme. It is worth to point out that others 3D anisotropic BEM formulations have also been recently proposed as, among others, those by [Wang and Denda (2007)] or [Shiah, Tan, and Wang (2012)].

The integral Equation (1) can be written as follows:

$$\tilde{\mathbf{C}}\mathbf{u}(P) + \sum_{e=1}^{N_e} \left\{ \int_{\partial\Omega^e} \mathbf{T}^* \mathbf{u} dS \right\} = \sum_{e=1}^{N_e} \left\{ \int_{\partial\Omega^e} \mathbf{U}^* \mathbf{t} dS \right\} \quad (10)$$

in case of absence of body loads ($\mathbf{b} = \mathbf{0}$), where the boundary $\partial\Omega$ is divided into N_e elements, $\partial\Omega^e \in \partial\Omega$, so: $\partial\Omega = \bigcup_{e=1}^{N_e} \partial\Omega^e$ and $\bigcap_{e=1}^{N_e} \partial\Omega^e = \emptyset$.

The fields \mathbf{u} and \mathbf{t} are approximated over each element $\partial\Omega^e$ using shape functions, as a function of the nodal values (\mathbf{d}^e and \mathbf{p}^e): $\mathbf{u} \simeq \hat{\mathbf{u}} = \mathbf{N}\mathbf{d}^e$ and $\mathbf{t} \simeq \hat{\mathbf{t}} = \mathbf{N}\mathbf{p}^e$, being \mathbf{N} the shape functions approximation matrix.

After the discretization, the Equation (10) can be written as

$$\tilde{\mathbf{C}}_i \mathbf{u}_i + \sum_{j=1}^N \tilde{\mathbf{H}}_i^e \mathbf{d}^e = \sum_{j=1}^N \tilde{\mathbf{G}}_i^e \mathbf{p}^e \quad (11)$$

being: $\tilde{\mathbf{H}}_i^e = \int_{\partial\Omega^e} \mathbf{t}^* \mathbf{N} d\Gamma$, $\tilde{\mathbf{G}}_i^e = \int_{\partial\Omega^e} \mathbf{u}^* \mathbf{N} d\Gamma$, the integrals over the element e when the collocation point is the node i . Finally, the contribution for all i nodes can be

written together in matrix form to give the global system of equations,

$$\tilde{\mathbf{H}}\mathbf{d} = \tilde{\mathbf{G}}\mathbf{p} \tag{12}$$

where \mathbf{d} and \mathbf{p} are the displacements and tractions nodal vectors, respectively. Matrices $\tilde{\mathbf{G}}$ and $\tilde{\mathbf{H}}$ are constructed collecting the terms of matrices $\tilde{\mathbf{H}}_i^e$ and $\tilde{\mathbf{G}}_i^e$.

2.2 Micromechanical model for continuous FRP

The variation of fiber volume fraction has a considerable influence on the contact pressure distribution. Micromechanics allows to estimate the mechanical properties of composite materials from the known values of the fiber and the matrix. In the literature, very sophisticated numerical models [Dong and Atluri (2012, 2013)], that make it possible to take into account micromechanics in heterogeneous materials, can be found. Nevertheless, much more specific micromechanical approaches can be considered for continuous fiber-reinforced composites (see Fig. 1(a)). The simplest approach is the *rule of mixtures*, but it fails to represent some of the properties with reasonable accuracy. A modified and more accuracy micromechanical model was proposed by [Hopkins and Chamis (1988)] whose expressions are:

$$E_1 = E_{f1}\bar{V}_f + E_m\bar{V}_m \tag{13}$$

$$E_2 = \left(\frac{\sqrt{\bar{V}_f}}{E_{b2}} + \frac{1 - \sqrt{\bar{V}_f}}{E_m} \right)^{-1} \tag{14}$$

$$G_{12} = \left(\frac{\sqrt{\bar{V}_f}}{G_{b12}} + \frac{1 - \sqrt{\bar{V}_f}}{G_m} \right)^{-1} \tag{15}$$

$$G_{23} = \left(\frac{\sqrt{\bar{V}_f}}{G_{b23}} + \frac{1 - \sqrt{\bar{V}_f}}{G_m} \right)^{-1} \tag{16}$$

$$\nu_{12} = \bar{V}_f\nu_{f12} + \bar{V}_m\nu_m \tag{17}$$

$$\nu_{23} = \frac{E_2}{2G_{23}} - 1 \tag{18}$$

being

$$E_{b2} = \sqrt{\bar{V}_f}E_{f2} + (1 - \sqrt{\bar{V}_f})E_m \tag{19}$$

$$G_{b12} = \sqrt{\bar{V}_f}G_{f12} + (1 - \sqrt{\bar{V}_f})G_m \tag{20}$$

$$G_{b23} = \sqrt{\bar{V}_f}G_{f23} + (1 - \sqrt{\bar{V}_f})G_m \tag{21}$$

In the expression above, \bar{V} is the volume fraction, and the subscripts f and m indicate the fiber and matrix, respectively.

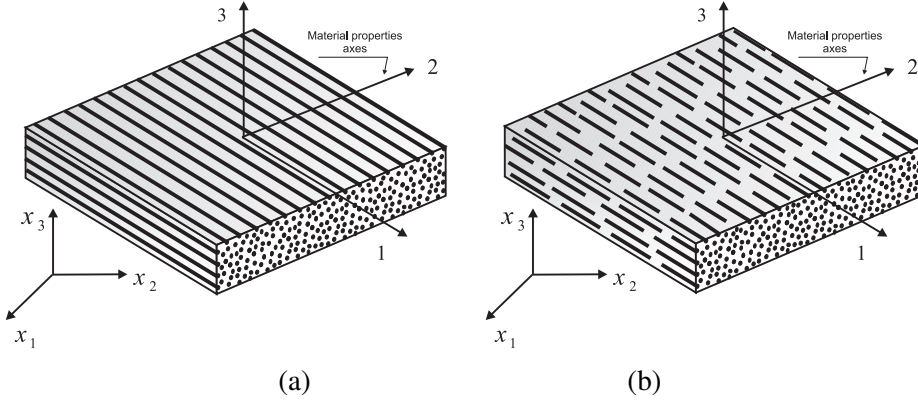


Figure 1: Example of two transversely isotropic composite materials: (a) continuous fiber-reinforced composite and (b) short fiber-reinforced composite.

2.3 Micromechanical model for short FRP

The Halpin-Tsai semi-empirical equations have long been applied to predict the properties of short-fiber composites (see Fig. 1(b)). A detailed review of their derivation is given in [Halpin and Kardos (1976)]. In the general form, the Halpin-Tsai equations for oriented reinforcements are written as

$$\frac{P}{P_m} = \frac{1 + \zeta \eta \bar{V}_f}{1 - \eta \bar{V}_f} \quad (22)$$

with

$$\eta = \frac{(P_f/P_m) - 1}{(P_f/P_m) + \zeta} \quad (23)$$

In the expressions above, P represents any one of the composite moduli (E_1 , E_2 , G_{12} , G_{23} and ν_{23}), and P_f and P_m are the corresponding moduli of the fibers (E_f , G_f and ν_f) and matrix (E_m , G_m and ν_m), while P is a parameter that depends on the matrix Poisson ratio and on the particular elastic property being considered. P was correlated with the geometry of the fiber and, when calculating E_1 , it should vary from some small value to infinity as a function of the fiber aspect ratio (l/d):

$$\zeta = 2 \frac{l}{d} + 40 \bar{V}_f^{10} \quad (24)$$

where l and d are the fiber length and diameter, respectively. It can be noted that for oriented continuous fiber-reinforced composites, $\zeta \rightarrow \infty$, and substitution of η into the Halpin-Tsai equation for E_1 gives the same result as the rule of mixture.

A modification for the Halpin-Tsai equation was proposed by [Nielsen (1974)], to include the maximum packing fraction, $\bar{V}_{f,max}$:

$$\frac{P}{P_m} = \frac{1 + \zeta \eta \bar{V}_f}{1 - \psi(\bar{V}_f) \eta \bar{V}_f} \tag{25}$$

where

$$\psi(\bar{V}_f) = 1 + \left(\frac{1 - \bar{V}_{f,max}}{\bar{V}_{f,max}^2} \right) \bar{V}_f \tag{26}$$

In case of fibrous reinforcements are arranged in a square array $\bar{V}_{f,max} = 0.785$. If they are arranged in a hexagonal array, $\bar{V}_{f,max} = 0.906$, and if they are arranged in random close packing, $\bar{V}_{f,max} = 0.82$.

3 Contact modeling

3.1 Kinematic equation

The contact problem between two linear anisotropic elastic bodies Ω^α , $\alpha = 1, 2$ with boundary $\partial\Omega^\alpha$ defined in the Cartesian coordinate system $\{x_i\}$ in \mathbb{R}^3 is considered (see Fig. 2). In order to know the relative position between both bodies at all times (τ), a gap variable is defined for the pair $I \equiv \{P^1, P^2\}$ of points ($P^\alpha \in \partial\Omega^\alpha$, $\alpha = 1, 2$), as $\mathbf{g} = \mathbf{B}^T(\mathbf{x}^2 - \mathbf{x}^1)$, where \mathbf{x}^α is the position of P^α at every instant. The position \mathbf{x}^α is defined as $\mathbf{x}^\alpha = \mathbf{X}^\alpha + \mathbf{u}_o^\alpha + \mathbf{u}^\alpha$, being \mathbf{X}^α the global position, \mathbf{u}_o^α the body Ω^α translation, and \mathbf{u}^α the small elastic displacement expressed in the global system. Matrix $\mathbf{B} = [\mathbf{t}_1 | \mathbf{t}_2 | \mathbf{n}]$, is a base change matrix expressing the pair I gap in relation to the local orthonormal base $\{\mathbf{t}_1, \mathbf{t}_2, \mathbf{n}\}$ associated to every I pair. The unitary vector \mathbf{n} is normal to the contact surfaces with the same direction as the normal to $\partial\Omega^1$ and expressed in the global system. Vectors $\{\mathbf{t}_1, \mathbf{t}_2\}$ are the tangential unitarian vectors (see Fig. 2).

The expression for the gap (\mathbf{g}) can be written as: $\mathbf{g} = \mathbf{B}^T(\mathbf{X}^2 - \mathbf{X}^1) + \mathbf{B}^T(\mathbf{u}_o^2 - \mathbf{u}_o^1) + \mathbf{B}^T(\mathbf{u}^2 - \mathbf{u}^1)$, being $\mathbf{B}^T(\mathbf{X}^2 - \mathbf{X}^1)$ the *geometric gap* between two solids in the reference configuration (\mathbf{g}_g), and $\mathbf{B}^T(\mathbf{u}_o^2 - \mathbf{u}_o^1)$ the gap originated due to the *rigid body movements* (\mathbf{g}_o). Therefore, the gap of the I pair remains as follows:

$$\mathbf{g} = \mathbf{g}_{g_o} + \mathbf{B}^T(\mathbf{u}^2 - \mathbf{u}^1) \tag{27}$$

where $\mathbf{g}_{g_o} = \mathbf{g}_g + \mathbf{g}_o$. In this work, the reference configuration for each solid (\mathbf{X}^α) that will be considered is the initial configuration (before applying load). Consequently, \mathbf{g}_g may also be termed *initial geometric gap*. In the expression (27) two components can be identified: the normal gap, $g_n = g_{g_o,n} + u_n^2 - u_n^1$, and the tangential gap or *slip*, $\mathbf{g}_t = \mathbf{g}_{g_o,t} + \mathbf{u}_t^2 - \mathbf{u}_t^1$, being u_n^α and $\mathbf{u}_t^\alpha = [u_{t1}^\alpha, u_{t2}^\alpha]$ the normal and tangential components of the displacements.

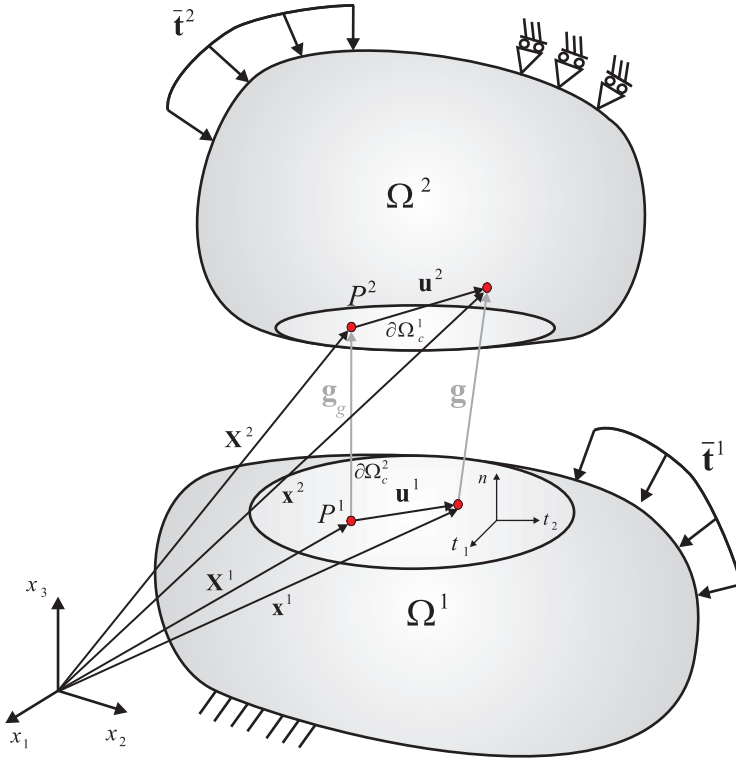


Figure 2: Contact pair I of points $P^\alpha \in \partial\Omega^\alpha$ ($\alpha = 1, 2$).

3.2 Normal contact law

The normal contact law involves two conditions ([Wriggers (2002)] and [Laursen (2002)]): impenetrability and no cohesion. The solids Ω^α ($\alpha = 1, 2$) are in contact without cohesion, if they can be separated. Therefore for each pair $I \equiv \{P^1, P^2\} \in \partial\Omega_c$ (*Contact Zone* $\partial\Omega_c$): $g_n \geq 0$ and $t_n \leq 0$. The variable g_n is the pair I normal gap, and t_n is the normal contact traction defined as: $t_n = \mathbf{B}_n^T \mathbf{t}^1 = -\mathbf{B}_n^T \mathbf{t}^2$, where \mathbf{t}^α is the traction at point $P^\alpha \in \Gamma_c^\alpha$ expressed in the global system of reference, and $\mathbf{B}_n = [\mathbf{n}]$ is the third column in the change of base matrix: $\mathbf{B} = [\mathbf{B}_t | \mathbf{B}_n] = [\mathbf{t}_1 | \mathbf{t}_2 | \mathbf{n}]$, vectors $\{\mathbf{t}_1, \mathbf{t}_2\}$ being parallel to the tribological axes $\{\mathbf{e}_1, \mathbf{e}_2\}$, respectively ($\beta = 0^\circ$, see Fig. 3(a)). Tangential traction is defined as: $\mathbf{t}_t = \mathbf{B}_t^T \mathbf{t}^1 = -\mathbf{B}_t^T \mathbf{t}^2$. Both tractions, \mathbf{t}^1 and \mathbf{t}^2 have the same value and opposite signs, in accordance with Newton's third law.

Finally, the variables g_n and t_n are complementary: $g_n t_n = 0$, so this set of relations may be summarized on $\partial\Omega_c$ by the so-called Signorini conditions:

$$g_n \geq 0, \quad t_n \leq 0, \quad g_n t_n = 0 \tag{28}$$

which have to be satisfied at every instant τ .

3.3 Anisotropic friction law

Experimental observations concerned with the directional sliding effects in anisotropic friction were provided by [Rabinowicz (1957)], [Halaunbrenner (1960)], and [Minford and Prewo (1985)]. Then theoretical investigations on friction surfaces and sliding rules were carried out by [Mróz and Stupkiewicz (1994)] [Zmitrowicz (1989, 1999)]. Their studies show that, in general, cross sections of the friction cone could be non-convex. However, in many engineering applications, a family of orthotropic friction models can be accurately approximated by a convex elliptical friction cone, where the principal axes of the ellipse coincide with the orthotropic axes. This is the case of FRP materials.

The form of such orthotropic limit friction is given by

$$f(\mathbf{t}_t, t_n) = \|\mathbf{t}_t\|_\mu - |t_n| = 0 \tag{29}$$

where $\|\bullet\|_\mu$ denotes the elliptic norm

$$\|\mathbf{t}_t\|_\mu = \sqrt{\left(\frac{t_{e1}}{\mu_1}\right)^2 + \left(\frac{t_{e2}}{\mu_2}\right)^2} \tag{30}$$

and the coefficients μ_1 and μ_2 are the principal friction coefficients. Curve (29) constitutes an ellipse whose principal axes are: $\mu_1|t_n|$ and $\mu_2|t_n|$ (see Fig. 3). The classical isotropic Coulomb's friction criterion is recovered on curve (29) considering $\mu_1 = \mu_2 = \mu$. The allowable contact tractions \mathbf{t} must satisfy: $f(\mathbf{t}_t, t_n) \leq 0$, defining an admissible convex region for \mathbf{t} : the *Friction Cone* (C_f).

An associated sliding rule is considered, so the sliding direction is given by the gradient to the friction cone and its magnitude by the factor λ :

$$\dot{g}_{e1} = -\lambda \frac{\partial f}{\partial t_{t1}} \quad \dot{g}_{e2} = -\lambda \frac{\partial f}{\partial t_{t2}} \tag{31}$$

To satisfy the complementarity relations

$$f(\mathbf{t}_t, t_n) \leq 0, \quad \lambda \geq 0, \quad \lambda f(\mathbf{t}_t, t_n) = 0 \tag{32}$$

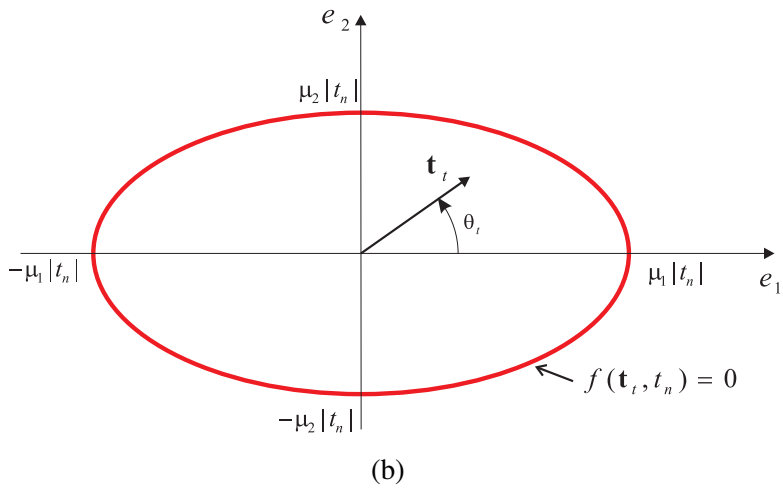
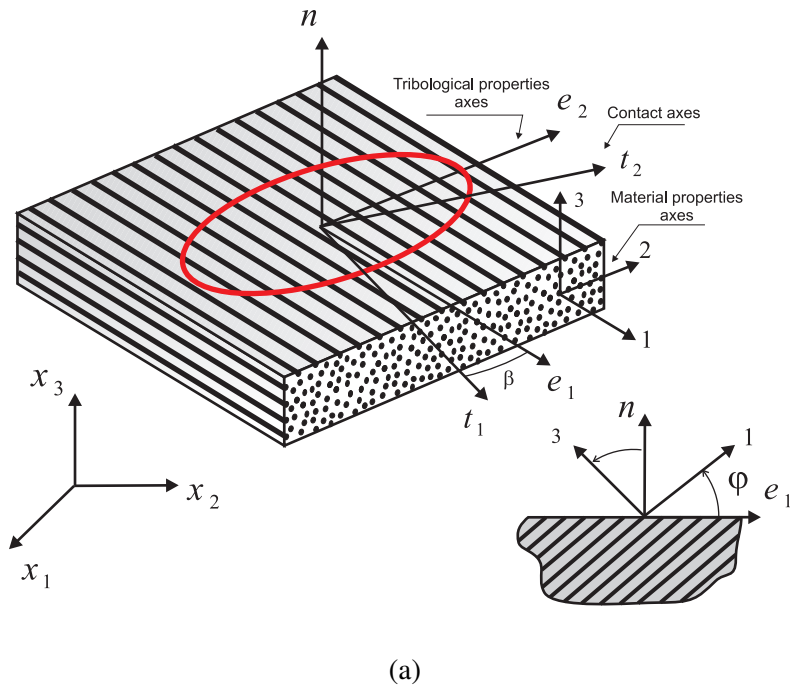


Figure 3: (a) Orthotropic surface with parallel fibers. (b) Elliptic friction law.

the expression for λ factor is: $\lambda = \|\dot{\mathbf{g}}_t\|_\mu^*$, where the norm $\|\bullet\|_\mu^*$ is dual of $\|\bullet\|_\mu$, so: $\|\dot{\mathbf{g}}_t\|_\mu^* = \sqrt{(\mu_1 \dot{g}_{e_1})^2 + (\mu_2 \dot{g}_{e_2})^2}$. Thus the components of \mathbf{t}_t are:

$$t_{e_1} = -\|\mathbf{t}_t\|_\mu \frac{\mu_1^2 \dot{g}_{e_1}}{\|\dot{\mathbf{g}}_t\|_\mu^*} \quad t_{e_2} = -\|\mathbf{t}_t\|_\mu \frac{\mu_2^2 \dot{g}_{e_2}}{\|\dot{\mathbf{g}}_t\|_\mu^*} \quad (33)$$

The Principle of Maximum Dissipation states that for solids in contact, the tangential traction (\mathbf{t}_t) in the slip zone is the one traction that maximizes the rate of energy dissipation, so the work done by the tangential contact tractions over the tangential slip has to be minimized: $W_d = t_{e_1} \dot{g}_{e_1} + t_{e_2} \dot{g}_{e_2} = -\lambda \|\mathbf{t}_t\|_\mu \Rightarrow W_d \leq 0$. So, in the contact-slip region ($f(\mathbf{t}_t, t_n) = 0$), the tangential traction satisfies

$$t_{e_1} = \frac{\partial W_d}{\partial \dot{g}_{e_1}} = -|t_n| \frac{\mu_1^2 \dot{g}_{e_1}}{\|\dot{\mathbf{g}}_t\|_\mu^*} \quad t_{e_2} = \frac{\partial W_d}{\partial \dot{g}_{e_2}} = -|t_n| \frac{\mu_2^2 \dot{g}_{e_2}}{\|\dot{\mathbf{g}}_t\|_\mu^*} \quad (34)$$

t_{e_α} and \dot{g}_{e_α} ($\alpha = 1, 2$) having opposite signs.

3.4 Contact restrictions

For any pair $I \equiv \{P^1, P^2\} \in \partial\Omega_c$ of points in contact, the *unilateral contact condition* and the *elliptic friction law* defined in the previous subsections can be compiled as follows, according to their contact status:

- No contact:

$$t_n = 0, \quad g_n \geq 0, \quad \mathbf{t}_t = \mathbf{0} \quad (35)$$

- Contact-Adhesion:

$$t_n \leq 0, \quad g_n = 0, \quad \dot{\mathbf{g}}_t = \mathbf{0} \quad (36)$$

- Contact-Slip:

$$t_n \leq 0, \quad g_n = 0, \quad \mathbf{t}_t = -|t_n| \mathbb{M}^2 \dot{\mathbf{g}}_t / \|\dot{\mathbf{g}}_t\|_\mu^* \quad (37)$$

being

$$\mathbb{M} = \begin{bmatrix} \mu_1 & 0 \\ 0 & \mu_2 \end{bmatrix} \quad (38)$$

In the expressions above, $\dot{\mathbf{g}}_t$ is the tangential slip velocity which can be expressed at time τ_k as: $\dot{\mathbf{g}}_t \simeq \Delta \mathbf{g}_t / \Delta \tau$, where $\Delta \mathbf{g}_t = \mathbf{g}_t(\tau_k) - \mathbf{g}_t(\tau_{k-1})$ and $\Delta \tau = \tau_k - \tau_{k-1}$,

according to a standard backward Euler scheme. So the constraints of the combined normal-tangential contact problem can be finally formulated as

$$\mathbf{t} - \mathbb{P}_{\mathbb{C}_f}(\mathbf{t}^*) = \mathbf{0} \quad (39)$$

where the contact operator $\mathbb{P}_{\mathbb{C}_f}$ is defined as

$$\mathbb{P}_{\mathbb{C}_f}(\mathbf{t}^*) = \left\{ \begin{array}{l} \mathbb{P}_{\mathbb{E}_\rho}(\mathbf{t}_t^*) \\ \mathbb{P}_{\mathbb{R}_-}(t_n^*) \end{array} \right\} \quad (40)$$

The normal projection function, $\mathbb{P}_{\mathbb{R}_-}(\cdot) : \mathbb{R} \longrightarrow \mathbb{R}_-$, is defined as

$$\mathbb{P}_{\mathbb{R}_-}(x) = \min(x, 0) \quad (41)$$

and the tangential projection function, $\mathbb{P}_{\mathbb{E}_\rho}, \mathbb{P}_{\mathbb{E}_\rho}(\cdot) : \mathbb{R}^2 \longrightarrow \mathbb{R}^2$,

$$\mathbb{P}_{\mathbb{E}_\rho}(\mathbf{x}) = \left\{ \begin{array}{ll} \mathbf{x} & \text{if } \|\mathbf{x}\|_\mu < \rho \\ \rho \mathbf{e}_t & \text{if } \|\mathbf{x}\|_\mu \geq \rho \quad (\mathbf{e}_t = \mathbf{x}/\|\mathbf{x}\|_\mu) \end{array} \right. \quad (42)$$

with $\mathbb{E}_\rho = \{\mathbf{x} \in \mathbb{R}^2 : \|\mathbf{x}\|_\mu - \rho = 0\}$ ($\rho = |\mathbb{P}_{\mathbb{R}_-}(t_n^*)|$). The augmented traction components $(\mathbf{t}^*)^T = [(t_t^*)^T t_n^*]$ are defined as:

$$\mathbf{t}_t^* = \mathbf{t}_t - r_t \mathbb{M}^2 \Delta \mathbf{g}_t \quad t_n^* = t_n + r_n g_n \quad (43)$$

being r_n and r_t the normal and tangential dimensional penalization parameters ($r_n \in \mathbb{R}^+, r_t \in \mathbb{R}^+$), respectively.

4 Solution procedure

4.1 Contact discrete variables

To consider the contact between two solids, the contact tractions (\mathbf{t}_c), the gap (\mathbf{g}), and the solids displacements (\mathbf{u}^α , $\alpha = 1, 2$), are discretized over the contact interface ($\partial\Omega_c$). To that end, $\partial\Omega_c$ is divided into N_e^f elemental surfaces ($\partial\Omega_c^e$), thus: $\partial\Omega_c = \bigcup_{e=1}^{N_e^f} \partial\Omega_c^e$; $\bigcap_{e=1}^{N_e^f} \partial\Omega_c^e = \emptyset$. These elements ($\partial\Omega_c^e$) constitute a *contact frame*.

The contact tractions are discretized over the contact frame as: $\mathbf{t}_c \simeq \hat{\mathbf{t}}_c = \sum_{i=1}^{N_e^f} \delta_{P_i} \lambda_i$ where δ_{P_i} is the Dirac's delta on each contact frame node i , and λ_i is the Lagrange multiplier on the node ($i = 1 \dots N_e^f$). The gap (\mathbf{g}) is approximated in the same way: $\mathbf{g} \simeq \hat{\mathbf{g}} = \sum_{i=1}^{N_e^f} \delta_{P_i} \mathbf{k}_i$, where \mathbf{k}_i is the nodal value.

The discrete expression of equation (27) can be written as:

$$\mathbf{k} = \mathbf{C}_g \mathbf{k}_{go} + (\mathbf{C}^2)^T \mathbf{x}^2 - (\mathbf{C}^1)^T \mathbf{x}^1 \tag{44}$$

being \mathbf{k} the contact pairs gap vector and \mathbf{k}_{go} the initial geometrical gap and rigid body movement vector. The matrices \mathbf{C}^α ($\alpha = 1, 2$) and \mathbf{C}_g were defined in [Rodríguez-Tembleque and Abascal (2010b)].

4.2 BE contact discrete equations

Equation (12) can be written for contact problems as: $\mathbf{A}_x \mathbf{x} + \mathbf{A}_p \mathbf{p}_c = \mathbf{f}$, being $(\mathbf{x})^T = [(\mathbf{x}_q)^T (\mathbf{d}_d)^T]$ the nodal unknowns vector that collects the external unknowns (\mathbf{x}_q), and the contact nodal displacements (\mathbf{d}_d). \mathbf{p}_c is the nodal contact tractions. \mathbf{A}_p is constructed with the columns of $\tilde{\mathbf{G}}$ belonging to the contact nodal unknowns, and $\mathbf{A}_x = [\mathbf{A}_x \mathbf{A}_d]$ with the columns matrices $\tilde{\mathbf{H}}$ and $\tilde{\mathbf{G}}$, corresponding to the exterior unknowns (\mathbf{A}_x), and the contact nodal displacements (\mathbf{A}_d).

Considering a boundary element discretization for every solid Ω^α ($\alpha = 1, 2$), the resulting BEM-BEM non-linear contact equations set can be expressed according with [Rodríguez-Tembleque and Abascal (2010a,b, 2013)], as

$$\begin{bmatrix} \mathbf{A}_x^1 & \mathbf{0} & \mathbf{A}_p^1 \tilde{\mathbf{C}}^1 & \mathbf{0} \\ \mathbf{0} & \mathbf{A}_x^2 & -\mathbf{A}_p^2 \tilde{\mathbf{C}}^2 & \mathbf{0} \\ (\mathbf{C}^1)^T & -(\mathbf{C}^2)^T & \mathbf{0} & \mathbf{C}_g \\ \mathbf{0} & \mathbf{0} & \mathbf{P}_\lambda & \mathbf{P}_g \end{bmatrix} \begin{bmatrix} \mathbf{x}^1 \\ \mathbf{x}^2 \\ \Lambda \\ \mathbf{k} \end{bmatrix} = \begin{bmatrix} \mathbf{f}^1 \\ \mathbf{f}^2 \\ \mathbf{C}_g \mathbf{k}_{go} \\ 0 \end{bmatrix} \tag{45}$$

The first two rows in the expression above represent the equilibrium of each solid Ω^α ($\alpha = 1, 2$). The third row is the contact kinematics equations and the last row express the nodal contact restrictions. Vector Λ represents the nodal contact tractions, so that: $\mathbf{p}_c^1 = \tilde{\mathbf{C}}^1 \Lambda$ and $\mathbf{p}_c^2 = -\tilde{\mathbf{C}}^2 \Lambda$. Matrices \mathbf{P}_λ and \mathbf{P}_g are the non-linear terms obtained by assembling the matrices $(\mathbf{P}_\lambda)_I$ and $(\mathbf{P}_g)_I$, associated to the I pair of nodes in contact. The values of the matrices depend on the I pair contact state:

- **No-Contact:** $(\Lambda_n^*)_I \geq 0$

$$(\mathbf{P}_\lambda)_I = \begin{bmatrix} 1 & 0 & 0 \\ 0 & 1 & 0 \\ 0 & 0 & 1 \end{bmatrix}_I, \quad (\mathbf{P}_g)_I = \begin{bmatrix} 0 & 0 & 0 \\ 0 & 0 & 0 \\ 0 & 0 & 0 \end{bmatrix}_I \tag{46}$$

- **Contact-Adhesion:** $(\Lambda_n^*)_I < 0$ and $\|(\Lambda_t^*)_I\|_\mu < |(\Lambda_n^*)_I|$

$$(\mathbf{P}_\lambda)_I = \begin{bmatrix} 0 & 0 & 0 \\ 0 & 0 & 0 \\ 0 & 0 & 0 \end{bmatrix}_I, \quad (\mathbf{P}_g)_I = \begin{bmatrix} -r_t \mu_1^2 & 0 & 0 \\ 0 & -r_t \mu_2^2 & 0 \\ 0 & 0 & -r_n \end{bmatrix}_I \tag{47}$$

- **Contact-Slip:** $(\Lambda_n^*)_I < 0$ and $\|(\Lambda_t^*)_I\|_\mu \geq |(\Lambda_n^*)_I|$

$$(\mathbf{P}_\lambda)_I = \begin{bmatrix} 1 & 0 & \omega_{t_1}^* \\ 0 & 1 & \omega_{t_2}^* \\ 0 & 0 & 0 \end{bmatrix}_I, \quad (\mathbf{P}_g)_I = \begin{bmatrix} 0 & 0 & 0 \\ 0 & 0 & 0 \\ 0 & 0 & -r_n \end{bmatrix}_I \quad (48)$$

being: $(\omega_t^*)_I = (\Lambda_t^*)_I / \|(\Lambda_t^*)_I\|_\mu$, and $(\Lambda_n^*)_I$ and $(\Lambda_t^*)_I$ the normal and tangential augmented variables components associated to the contact pair I : $(\Lambda_n^*)_I = (\Lambda_n)_I + r_n(\mathbf{k}_n)_I$ and $(\Lambda_t^*)_I = (\Lambda_t)_I + r_t \mathbb{M}^2(\mathbf{k}_t)_I$.

4.3 Solution scheme

To solve the system (45), $\mathbf{Rz} = \mathbf{F}$, the *Generalized Newton Method with Line Search* (GNMLS) can be applied over: $\Theta(\mathbf{z}) = \mathbf{Rz} - \mathbf{F} = \mathbf{0}$. The GNMLS is an effective extension of the Newton's method for \mathcal{B} -differentiable functions proposed by [Pang (1990)] in a general context and particularized by [Alart (1997)] and [Christensen, Klarbring, Pang, and Strömberg (1998)] for contact problems. This method can be summarized in the following steps:

- (1) Start iteration, loop n , defining an arbitrary initial vector $\mathbf{z}^{(0)}$, and the positive scalars: $q > 0$, $\beta \in (0, 1)$, $\sigma \in (0, 1/2)$, and $\varepsilon > 0$.
- (2) Solve for $\Delta\mathbf{z}^{(n)}$, the system $\mathcal{B}\Theta(\mathbf{z}^{(n)}, \Delta\mathbf{z}^{(n)}) = -\Theta(\mathbf{z}^{(n)})$, where $\mathcal{B}\Theta(\mathbf{z}^{(n)}, \Delta\mathbf{z}^{(n)})$ is the function \mathcal{B} -derivative.
- (3) Obtain first integer $m = 1, 2, \dots$ that fulfills the following decreasing error condition: $\Psi(\mathbf{z}^{(n)} + \alpha^{(n)} \Delta\mathbf{z}^{(n)}) \leq (1 - 2\sigma\alpha^{(n)}) \Psi(\mathbf{z}^{(n)})$, with $\alpha^{(n)} = \beta^m q$ and $\Psi(\mathbf{z}^{(n)}) = \frac{1}{2} \|\Theta(\mathbf{z}^{(n)})\|^2$.
- (4) Actualize solution: $\mathbf{z}^{(n+1)} = \mathbf{z}^{(n)} + \alpha^{(n)} \Delta\mathbf{z}^{(n)}$.
- (5) If $\Psi(\mathbf{z}^{(n+1)}) \leq \varepsilon$, the solution is achieved: $\mathbf{z}^{(n+1)}$, else compute new iteration ($n \leftarrow n + 1$).

In step 2, the \mathcal{B} -derivative can be approximated according with [Strömberg (1997)]: $\mathcal{B}\Theta(\mathbf{z}^{(n)}, \Delta\mathbf{z}^{(n)}) \simeq \mathbf{J}^{(n)} \Delta\mathbf{z}^{(n)}$, being

$$\mathbf{J}^{(n)} \Delta\mathbf{z}^{(n)} = \begin{bmatrix} \mathbf{R}^1 & \mathbf{R}^2 & \mathbf{R}_\lambda & \mathbf{R}_g \\ \mathbf{0} & \mathbf{0} & \mathbf{J}_\lambda^{(n)} & \mathbf{J}_g^{(n)} \end{bmatrix} \begin{Bmatrix} \Delta\mathbf{d}^1 \\ \Delta\mathbf{x}^2 \\ \Delta\Lambda \\ \Delta\mathbf{k} \end{Bmatrix}^{(n)} \quad (49)$$

Matrices $\mathbf{J}_\lambda^{(n)}$ and $\mathbf{J}_g^{(n)}$ are constructed from the assembly of the matrices associated to each I pair: $(\mathbf{J}_\lambda^{(n)})_I$ and $(\mathbf{J}_g^{(n)})_I$, which are associated to each I pair, like \mathbf{P}_λ and \mathbf{P}_g , and they were defined in [Rodríguez-Tembleque and Abascal (2010b)], according to the directional derivative presented in [Christensen, Klarbring, Pang, and Strömberg (1998)] for the B-differentiable Newton method. The value of these matrices depends on the I pair augmented contact variables states:

- No-Contact: $(\Lambda_n^{*(n)})_I \geq 0$

$$(\mathbf{J}_\lambda^{(n)})_I = \begin{bmatrix} 1 & 0 & 0 \\ 0 & 1 & 0 \\ 0 & 0 & 1 \end{bmatrix}_I \quad (\mathbf{J}_g^{(n)})_I = \begin{bmatrix} 0 & 0 & 0 \\ 0 & 0 & 0 \\ 0 & 0 & 0 \end{bmatrix}_I \quad (50)$$

- Contact-Adhesion: $(\Lambda_n^{*(n)})_I < 0$ and $\|(\Lambda_t^{*(n)})_I\|_\mu < |(\Lambda_n^{*(n)})_I|$

$$(\mathbf{J}_\lambda^{(n)})_I = \begin{bmatrix} 0 & 0 & 0 \\ 0 & 0 & 0 \\ 0 & 0 & 0 \end{bmatrix}_I \quad (\mathbf{J}_g^{(n)})_I = \begin{bmatrix} -r_t \mu_1^2 & 0 & 0 \\ 0 & -r_t \mu_2^2 & 0 \\ 0 & 0 & -r_n \end{bmatrix}_I \quad (51)$$

- Contact-Slip: $(\Lambda_n^{*(n)})_I < 0$ and $\|(\Lambda_t^{*(n)})_I\|_\mu \geq |(\Lambda_n^{*(n)})_I|$

$$(\mathbf{J}_\lambda^{(n)})_I = \begin{bmatrix} \Psi_{11} & \Psi_{12} & \omega_{t_1}^* \\ \Psi_{21} & \Psi_{22} & \omega_{t_2}^* \\ 0 & 0 & 0 \end{bmatrix}_I^{(n)} \quad (\mathbf{J}_g^{(n)})_I = \begin{bmatrix} -r_t \tilde{\Psi}_{11} & -r_t \tilde{\Psi}_{12} & 0 \\ -r_t \tilde{\Psi}_{21} & -r_t \tilde{\Psi}_{22} & 0 \\ 0 & 0 & -r_n \end{bmatrix}_I^{(n)} \quad (52)$$

being: $\Psi = (1 + \phi)\mathbf{I} - \psi\mathbf{S}$, $\tilde{\Psi} = (\Psi - \mathbf{I})\mathbb{M}^2$, $\omega_t^{*(n)} = (\Lambda_t^{*(n)})_I / \|(\Lambda_t^{*(n)})_I\|_\mu$, $\mathbf{S} = [(\Lambda_t^{*(n)})_I \otimes (\Lambda_t^{*(n)})_I] \mathbb{M}^{-2}$, $\phi = (\Lambda_n^{*(n)})_I / \|(\Lambda_t^{*(n)})_I\|_\mu$, and $\psi = (\Lambda_n^{*(n)})_I / \|(\Lambda_t^{*(n)})_I\|_\mu^3$.

5 Numerical studies

The formulation presented above allows to study an indentation problem, where a carbon FRP is studied under different contact conditions. A steel sphere of radius $R = 50 \text{ mm}$ is indented on a carbon FRP half-space (see Fig. 4(a)). The sphere is subjected to a normal displacement $g_{o,x_3} = -0.02 \text{ mm}$ and a tangential translational displacement of module: $g_{o,t} = 0.001 \text{ mm}$, which forms an angle θ with axis x_1 . The carbon FRP considered is IM7 Carbon/ 8551 - 7, whose mechanical properties of its fiber and matrix can be found in Kaddour and Hinton (2012) (Tab. 1). An

Table 1: Mechanical properties of fiber and matrix.

Fiber	IM7
Longitudinal Young modulus E_{f1} (GPa)	276
Transverse Young modulus E_{f2} (GPa)	19
Transverse Young modulus E_{f3} (GPa)	19
In-plane shear modulus G_{f12} (GPa)	27
Transverse shear modulus G_{f23} (GPa)	7
Poisson ratio ν_{f12}	0.2
Poisson ratio ν_{f13}	0.2
Matrix	8551 – 7 epoxy
Elastic modulus E_m (GPa)	4.08
Elastic shear modulus G_m (GPa)	1.478
Poisson ratio ν_m	0.38

orthotropic friction law is considered, being the friction coefficients: $\mu_1 = 0.1$ and $\mu_2 = 0.2$.

For simplicity, due to the contact half-width (a) will be much less than the radius (R), the solids are approximated by elastic half-spaces, each one discretized using linear quadrilateral boundary elements. Fig. 4(b) shows the meshes details, where the half-space characteristic dimension is $L = 1.2 \text{ mm}$.

5.1 Influence of fiber orientation and volume fraction

In this indentation problem, the influence of fiber orientation and fiber volume fraction in the contact variables is considered. Figures 5(a) and (b), show the normal and tangential contact compliance variation with the fiber orientation, relative to the load for the fiber alignment parallel to the axe x_1 ($\varphi = 0$) and a volume fraction of 30 %. For the normal load (Fig. 5(a)), the largest loads occur in the normal fiber orientation ($\varphi = 90^\circ$), and high differences can be observed for φ greater than 45° . For the tangential contact compliance (5(b)), with $\theta = 0^\circ$, the variation relative to the load $Q(\varphi = 0)$ presents a different behavior. The largest loads does not occur in the normal fiber orientation, but occurs for an orientation in the interval $[30^\circ, 60^\circ]$ for the carbon FRP. Examining the Fig. 6, it is found that the variation of the orientation of the fibers has and important effect on the magnitude of the normal contact pressure. The maximum value of normal pressure increases with φ , but the contact width remains constant with the variation on the fiber alignment.

The variation of fiber volume fraction has also a considerable influence on the contact problem. Considering a continuous fiber micromechanical model, the influence

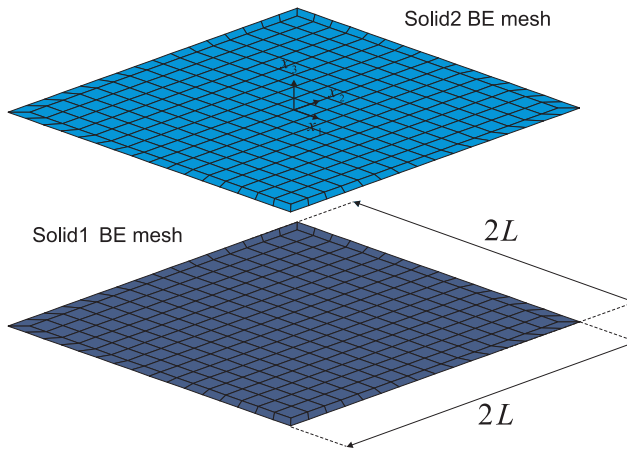
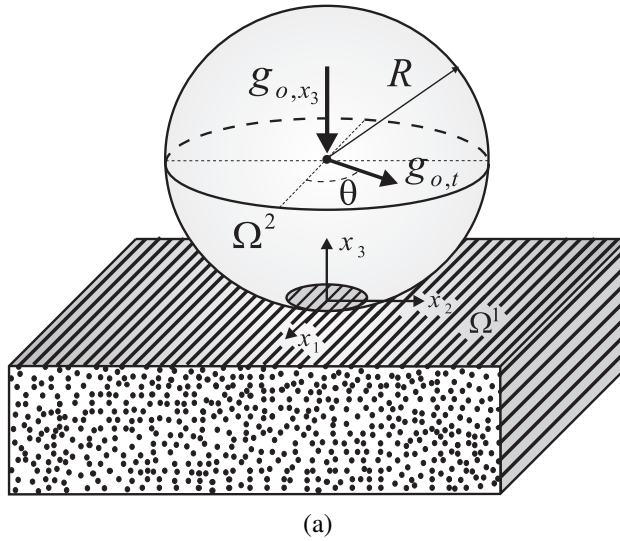
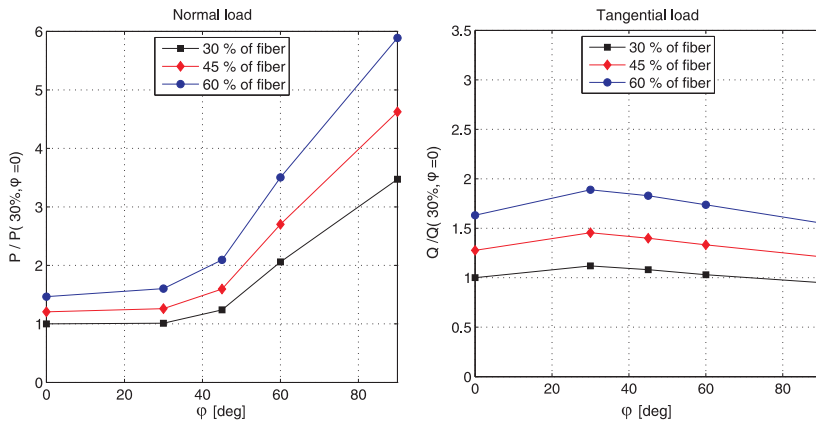


Figure 4: (a) Sphere indentation over a FRP halfspace. (b) Boundary elements mesh details.



(b)

Figure 5: Influence of the fiber volume fraction on the normal (a) and tangential (b) contact compliance, for a continuous FRP micromechanical model.

of fiber volume fraction \bar{V}_f has been also studied for $\bar{V}_f = \{0.30, 0.45, 0.60\}$. Figures 5(a) and (b) shows the influence of the fiber volume fraction on the normal and tangential contact loads, for a fixed normal indentation and tangential translational displacement. For every fiber orientation, the normal load increases its value with \bar{V}_f , but the biggest increment occurs in the normal fiber orientation. Same behavior is observed in Fig. 5(b) for the tangential load: its value increases with \bar{V}_f .

The convergence of the proposed approach is illustrated in Fig. 7 where the relative error evolution for a fiber volume fraction $\bar{V}_f = 0.6$ is showed. Different fiber orientations (Fig. 7 (a)) and different sliding directions (Fig. 7 (b)) are considered. In all these cases, the convergence criteria is $\varepsilon = 10^{-3}$. It can be observed that the algorithm is efficient and presents a similar rate of convergence in all the cases studied.

5.2 Influence of fiber length

Same studies as in Section 2.3 are presented here for short carbon fibers ($l/d = 10$), considering the Halpin-Tsai's micromechanical model. In Fig. 8 it can be observed that short fibers contact compliances present the same tendency than continuous fibers compliances when the fiber orientation and/or volume fraction is modified. The influence of fiber length is presented in Fig. 9, where the normal and tangential contact compliance for continuous and short fiber-reinforced micromechanical models are compared. Short fibers present a lower normal contact compliance than

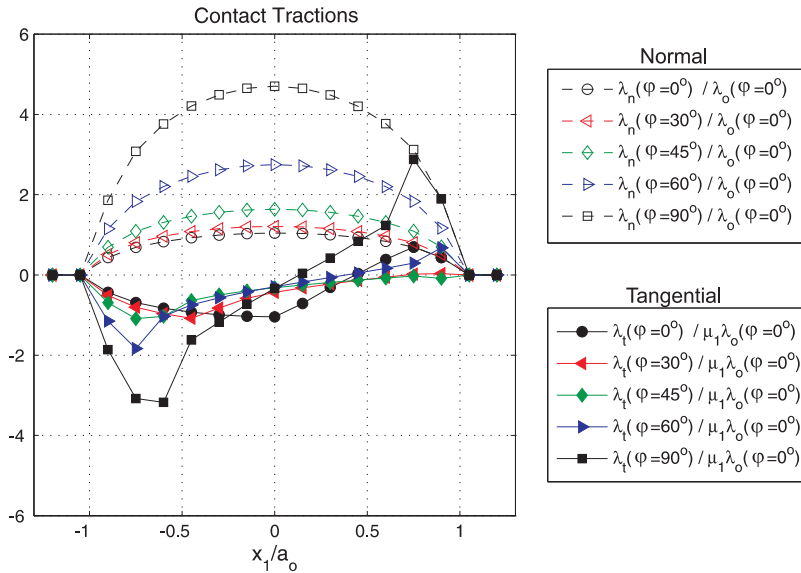


Figure 6: Influence of fiber orientation on the contact tractions distribution for IM7 Carbon/ 8551 – 7 ($\bar{V}_f = 0.6$).

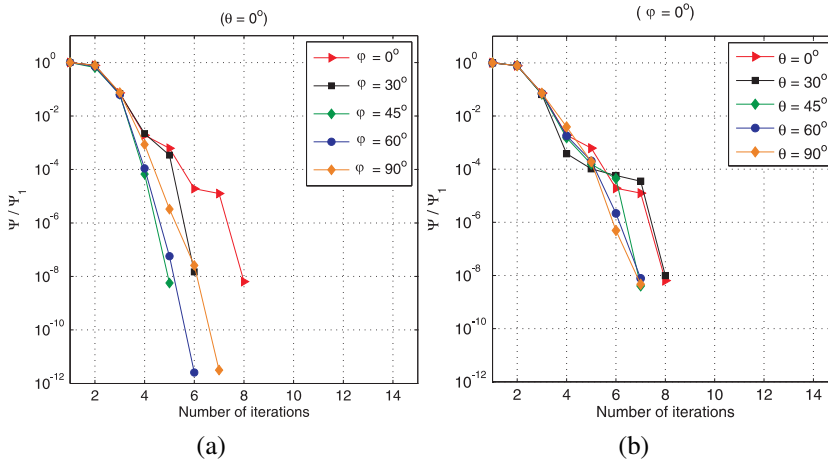


Figure 7: Error evolution for the sphere indentation over a FRP halfspace considering different: (a) fiber orientations and (b) sliding directions.

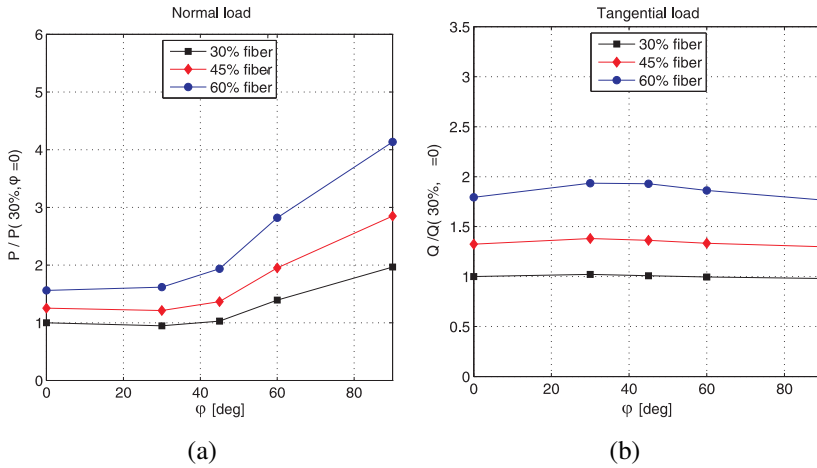


Figure 8: Influence of the fiber volume fraction on the normal (a) and tangential (b) contact compliance, for a short FRP micromechanical model ($l/d = 10$).

continuous fibers when the fiber orientation is normal to the surface. For the tangential contact compliance, the largest difference between short-fibers and continuous ones occurs for fiber orientation in the interval $[30^\circ, 60^\circ]$.

5.3 Influence of sliding direction

Finally, the influence of sliding direction may be analyzed by considering $\theta = \{0^\circ, 30^\circ, 45^\circ, 60^\circ, 90^\circ\}$. Fig. 10(a) shows the tangential load variation, relative to the load $Q(\varphi = 0)$, also taking into account the influence of fiber orientation. If the sliding direction is parallel to the fiber direction ($\theta = 0^\circ$), the tangential compliance presents a maximum for the fiber orientation interval: $[30^\circ, 60^\circ]$. Fig. 10 (b) shows the influence of the fiber volume fraction on the orthotropic tangential contact compliance for a fixed fiber orientation ($\varphi = 0^\circ$). For every sliding direction θ , the tangential load increases in the same proportion with \bar{V}_f .

6 Summary and conclusions

This work presents a boundary element methodology which allows us to analyze polymer composites under frictional contact conditions, taking into account both the mechanical and the tribological anisotropic characteristics. Using this numerical formulation a carbon FRP have been analyzed, under different contact conditions. In these studies, the influence of fiber orientation, fiber length, sliding

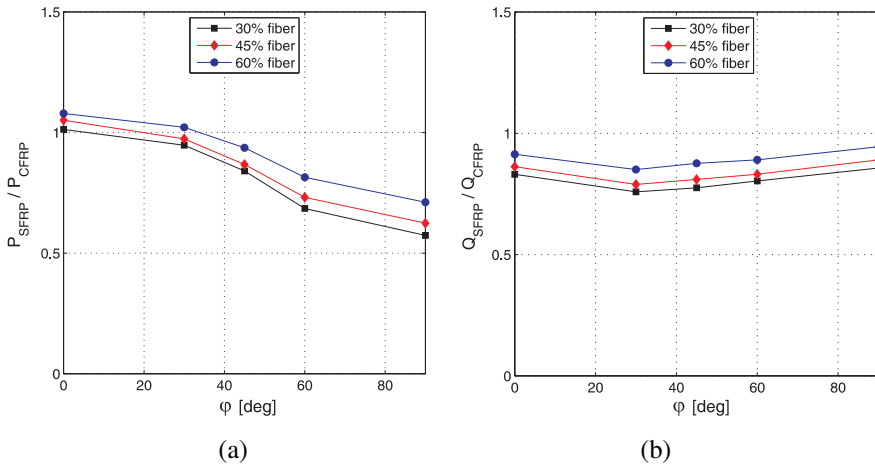


Figure 9: Normal contact compliance (a) and tangential contact compliance (b) comparison between continuous FRP (CFRP) and short FRP (SFRP) micromechanical models.

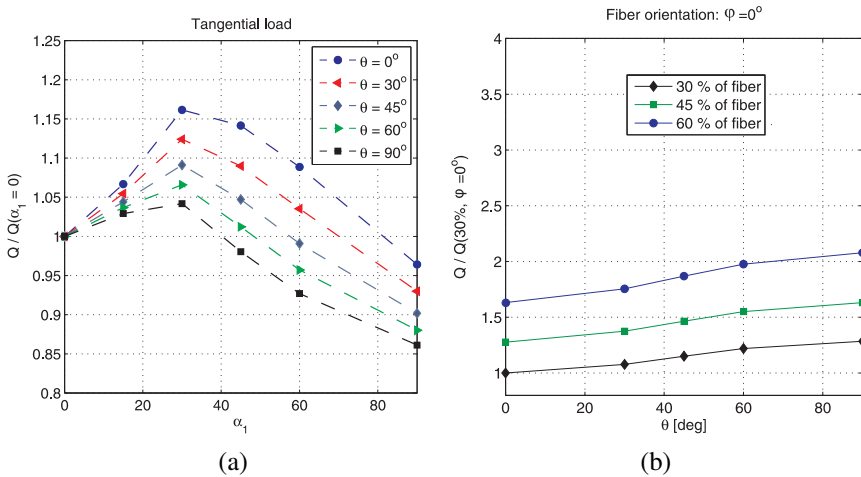


Figure 10: (a) Influence of sliding direction on the tangential load for IM7 Carbon/8551 – 7 ($\bar{V}_f = 0.6$). (b) Influence of the fiber volume fraction on the orthotropic tangential contact compliance.

direction or fiber volume fraction, over the contact variables, have been studied, considering a *sphere-half space* indentation problem.

All these examples show the importance of taking into account the influence of anisotropy and the micromechanics of the bulk, and the anisotropy of the surface properties, in contact problems between fiber-reinforced composites. Their influence on the contact variables is important, since contact traction distributions and contact compliances are clearly modified by the fiber orientation, the fiber length, the volume fraction or the sliding direction. In other case, we could over- or underestimate contact magnitudes and their distribution over the contact zone.

Acknowledgement: This work was co-funded by the DGICYT of *Ministerio de Ciencia y Tecnología*, Spain, research projects DPI2010-19331 and DPI2010-21590-C02-02, which were co-funded by the European Regional Development Fund (ERDF) (Fondo Europeo de Desarrollo Regional, FEDER).

References

Abascal, R.; Rodríguez-Tembleque, L. (2007): Steady-state 3d rolling-contact using boundary elements. *Commun. Numer. Meth. Engng.*, vol. 23, pp. 905–920.

Alart, P. (1997): méthode de newton généralisée en mécanique du contact. *J. Math. Pure Appl.*, vol. 76, pp. 83–108.

Alart, P.; Curnier, A. (1991): A mixed formulation for frictional contact problems prone to newton like solution methods. *Comput. Method. Appl. Mech. Eng.*, vol. 92, pp. 353–375.

Aliabadi, M. H. (2002): *The Boundary Element Method Vol2: Applications in Solids and Structures*. John Wiley & Sons.

Bagault, C.; Nélias, D.; Baietto, M. (2012): Contact analyses for anisotropic half space: Effect of the anisotropy on the pressure distribution and contact area. *J. Tribol.*, vol. 134, pp. 1–8.

Bagault, C.; Nélias, D.; Baietto, M.; Ovaert, T. (2013): Contact analyses for anisotropic half-space coated with an anisotropic layer: Effect of the anisotropy on the pressure distribution and contact area. *Int. J. Solids Struct.*, vol. 50, pp. 743–754.

Batra, R.; Jiang, W. (2008): Analytical solution of the contact problem of a rigid indenter and an anisotropic linear elastic layer. *Int. J. Solids Struct.*, vol. 45, pp. 5814–5830.

Brebbia, C. A.; Dominguez, J. (1992): *Boundary Elements: An Introductory Course (second edition)*. WIT Press.

Buroni, F.; Ortiz, J.; Sáez, A. (2011): Multiple pole residue approach for 3d bem analysis of mathematical degenerate and non-degenerate materials. *Int. J. Numer. Methods Eng.*, vol. 86, pp. 1125–1143.

Buroni, F.; Sáez, A. (2013): Unique and explicit formulas for green's function in three-dimensional anisotropic linear elasticity. *Journal of Applied Mechanics*, vol. 80, pp. 051018.

Christensen, P. W.; Klarbring, A.; Pang, J. S.; Strömberg, N. (1998): Formulation and comparison of algorithms for frictional contact problems. *Int. J. Numer. Meth. Eng.*, vol. 42, pp. 145–173.

Cirino, M.; Friedrich, K.; Pipes, R. B. (1988): The effect of fiber orientation on the abrasive wear behavior of polymer composite materials. *Wear*, vol. 121, pp. 127–141.

Dong, L.; Atluri, S. N. (2012): Development of 3D T-Trefftz Voronoi Cell Finite Elements with/without Spherical Voids and/or Elastic/Rigid Inclusions for Micromechanical Modeling of Heterogeneous Materials. *CMC: Computers Materials and Continua*, vol. 29, no. 2, pp. 169–211.

Dong, L.; Atluri, S. N. (2013): SGBEM Voronoi Cells (SVCs), with Embedded Arbitrary-Shaped Inclusions, Voids, and/or Cracks, for Micromechanical Modeling of Heterogeneous Materials. *CMC: Computers Materials and Continua*, vol. 33, no. 2, pp. 111–154.

Gladwell, G. (1980): *Contact problem in the classical theory of elasticity*. Sijthoff & Noordhoff. Alphen aan den Rijn.

Goda, T.; Váradi, K.; Wetzel, B.; Friedrich, K. (2004): Finite element simulation of the fiber–matrix debonding in polymer composites produced by a sliding indenter: Part i – normally oriented fibers. *J. Compos. Mater.*, vol. 38, pp. 1583–1606.

Goda, T.; Váradi, K.; Wetzel, B.; Friedrich, K. (2004): Finite element simulation of the fiber–matrix debonding in polymer composites produced by a sliding indenter: Part ii – parallel and anti-parallel fiber orientation. *J. Compos. Mater.*, vol. 38, pp. 1607–1618.

Graciani, E.; Mantic, V.; París, F.; Varna, J. (2009): Numerical analysis of debond propagation in the single fibre fragmentation test. *Compos. Sci. Technol.*, vol. 69, pp. 2514–2520.

Halaunbrenner, M. (1960): Direction of the friction forces. *Wear*, vol. 3, pp. 421–425.

Halpin, J.; Kardos, J. (1976): The halpin-tsai equations: a review. *Polym. Eng. Sci.*, vol. 16, pp. 344–352.

- Hopkins, D. A.; Chamis, C. C.** (1988): *A Unique Set of Micromechanics Equations for High Temperature Metal Matrix Composites. In: Testing Technology of Metal Matrix Composites, ASTM STP 964.*, American Society for Testing and Materials.
- Hwu, C.; Fan, C.** (1998): Sliding punches with or without friction along the surface of an anisotropic elastic half-plane. *Q. J. Mech. Appl. Math.*, vol. 51, pp. 159–177.
- Jacobs, O.; Friedrich, K.; Marom, G.; Schulte, K.; Wagner, H. D.** (1990): Fretting wear performance of glass-, carbon-, and aramid-fibre/ epoxy and peek composites. *Wear*, vol. 135, pp. 207–216.
- Jiang, W.; Batra, R.** (2010): Indentation of a laminated composite plate with an interlayer rectangular void. *Compos. Sci. Technol.*, vol. 70, pp. 1023–1030.
- Kaddour, A. S.; Hinton, M. J.** (2012): Input data for test cases used in benchmarking triaxial failure theories of composites. *J. Compos. Mater.*, vol. 54, pp. 2295–2312.
- Klarbring, A.** (1992): *Mathematical Programming and Augmented Lagrangian Methods for Frictional Contact Problems.* Proceedings of Contact Mechanics International Symposium. Presses Polytechniques et Universitaires Romandes, Lausanne.
- Klarbring, A.** (1993): *Mathematical programming in contact problems.* Computational methods in contact mechanics.
- Larsen, T.; Andersen, T. L.; Thorning, B.; Horsewell, A.; Vigild, M.** (2007): Fretting wear performance of glass-, carbon-, and aramid-fibre/ epoxy and peek composites. *Wear*, vol. 262, pp. 1013–1020.
- Laursen, T. A.** (2002): *Computational Contact and Impact Mechanics.* Springer, England.
- Lee, V.** (2003): Explicit expressions of derivatives of elastic greens functions for general anisotropic materials. *Mech. Res. Comm.*, vol. 30, pp. 241–249.
- Lovell, M.** (1998): Analysis of contact between transversely isotropic coated surfaces: development of stress and displacement relationships using fem. *Wear*, vol. 194, pp. 60–70.
- Mantic, V.; Graciani, E.; París, F.; Varna, J.** (2005): *An axisymmetric boundary element analysis of interface cracks in fiber reinforced composites. In: Advances in boundary element techniques, vol. VI.* Eastleigh: EC Ltd.
- Minford, E.; Prewo, K.** (1985): Friction and wear of graphite-fiber-reinforced glass matrix composites. *Wear*, vol. 102, pp. 253–264.

- Mróz, Z.; Stupkiewicz, S.** (1994): An anisotropic friction and wear model. *Int. J. Solids Struct.*, vol. 31, pp. 1113–1131.
- Nielsen, L.** (1974): *Mechanical properties of polymers and composites*. Marcel Dekker, New York.
- Ning, X.; Lovell, M. R.** (2002): On the sliding friction characteristics of unidirectional continuous frp composites. *J. Tribol.*, vol. 124, pp. 5–13.
- Ning, X.; Lovell, M. R.; Morrow, C.** (2004): Anisotropic strength approach for wear analysis of unidirectional continuous frp composites. *J. Tribol.*, vol. 126, pp. 65–70.
- Ning, X.; Lovell, M. R.; Slaughter, W. S.** (2006): Asymptotic solutions for axisymmetric contact of a thin, transversely isotropic elastic laye. *Wear*, vol. 260, pp. 693–698.
- Ohmae, N.; Kobayashi, K.; Tsukizoe, T.** (1974): Characteristics of fretting of carbon fibre reinforced plastics. *Wear*, vol. 29, pp. 345–353.
- Pang, J.** (1990): Newton’s method for b-differentiable equations. *Math. Oper. Research.*, vol. 15, pp. 311–341.
- Rabinowicz, E.** (1957): Directional effects in friction. *Nature*, vol. 179, pp. 1073.
- Rodríguez-Tembleque, L.; Abascal, R.** (2010): A 3d fem-bem rolling contact formulation for unstructured meshes. *Int. J. Solids Struct.*, vol. 47, pp. 330–353.
- Rodríguez-Tembleque, L.; Abascal, R.** (2010): A fem-bem fast methodology for 3d frictional contact problems. *Comput. Struct.*, vol. 88, pp. 924–937.
- Rodríguez-Tembleque, L.; Abascal, R.** (2013): Fast fe-bem algorithms for orthotropic frictional contact. *Int. J. Numer. Meth. Eng.*, vol. 94, pp. 687–707.
- Rodríguez-Tembleque, L.; Abascal, R.; Aliabadi, M. H.** (2010): A boundary element formulation for wear modeling on 3d contact and rolling-contact problems. *Int. J. Solids Struct.*, vol. 47, pp. 2600–2612.
- Rodríguez-Tembleque, L.; Abascal, R.; Aliabadi, M. H.** (2011): A boundary element formulation for 3d fretting-wear problems. *Engng. Anal. Bound. Elem.*, vol. 35, pp. 935–943.
- Rodríguez-Tembleque, L.; Abascal, R.; Aliabadi, M. H.** (2012): Anisotropic fretting wear simulation using the boundary element method. *CMES–Computer Modeling in Engineering and Sciences*, vol. 87, pp. 127–155.
- Rodríguez-Tembleque, L.; Abascal, R.; Aliabadi, M. H.** (2012): Anisotropic wear framework for 3d contact and rolling problems. *Comput. Meth. Appl. Mech. Eng.*, vol. 241, pp. 1–19.

Rodríguez-Tembleque, L.; Buroni, F. C.; Abascal, R.; Sáez, A. (2011): 3d frictional contact of anisotropic solids using bem. *Eur. J. Mech. A. Solids.*, vol. 30, pp. 95–104.

Scholz, M.; Blanchfield, J.; Bloom, L.; Coburn, B.; Elkington, M.; Fuller, J.; Gilbert, M.; Muffahi, S.; Pernice, M.; Rae, S.; Trevarthen, J.; White, S.; Weaver, P.; Bond, I. (2011): The use of composite materials in modern orthopaedic medicine and prosthetic devices: A review. *Composites Science and Technology*, vol. 16, pp. 1791–1803.

Shiah, Y. C.; Tan, C. L.; Wang, C. Y. (2012): Efficient computation of the green's function and its derivatives for three-dimensional anisotropic elasticity in bem analysis. *Engng. Anal. Bound. Elem.*, vol. 36, pp. 1746–1755.

Strömberg, N. (1997): An augmented lagrangian method for fretting problems. *Eur. J. Mech. A. Solids.*, vol. 16, pp. 573–593.

Sung, N. H.; Suh, N. P. (1979): Effect of fiber orientation on friction and wear of fiber reinforced polymeric composites. *Wear*, vol. 53, pp. 129–141.

Swadener, J.; Pharr, G. (2001): Indentation of elastically anisotropic half-spaces by cones and parabolae of revolution. *Philos. Mag. A.*, vol. 81, pp. 447–466.

Ting, T. (1996): *Anisotropic Elasticity*. Oxford University Press, Oxford.

Ting, T.; Lee, V. (1997): The three-dimensional elastostatic green's function for general anisotropic linear elastic solids. *Q. J. Mech. Appl. Math.*, vol. 50, pp. 407–426.

Tsukizoe, T.; Ohmae, N. (1983): Friction and wear of advanced composite materials. *Fibre Science and Technology*, vol. 18, pp. 265–286.

Turner, J. (1980): Contact on a transversely isotropic half-space, or between two transversely isotropic bodies. *Int. J. Solids Struct.*, vol. 16, pp. 409–419.

Vàradi, K.; Nèder, Z.; Flöck, J.; Friedrich, K. (1998): Numerical and experimental contact analysis of a steel ball indented into a fibre reinforced polymer composite material. *Journal of Materials Science*, vol. 33, pp. 841–851.

Vàradi, K.; Nèder, Z.; Friedrich, K.; Flöck, J. (1999): Finite-element analysis of a polymer composite subjected to a ball indentation. *Compos. Sci. Technol.*, vol. 59, pp. 271–281.

Vishwanath, B.; Verma, A. P.; Rao, V. S. K. (1993): Effect of reinforcement on friction and wear of fabric reinforced polymer composites. *Wear*, vol. 167, pp. 93–99.

Vlassak, J.; Ciavarella, M.; Barber, J.; Wang, X. (2003): The indentation modulus of elastically anisotropic materials for indenters of arbitrary shape. *J. Mech. Phys. Solids.*, vol. 51, pp. 1701–1721.

Vlassak, J.; Nix, W. (1993): Indentation modulus of elastically anisotropic half spaces. *Philos. Mag. A.*, vol. 67, pp. 1045–1056.

Vlassak, J.; Nix, W. (1994): Measuring the elastic properties of anisotropic materials by means of indentation experiments. *J. Mech. Phys. Solids.*, vol. 42, pp. 1223–1245.

Wang, C.; Denda, M. (2007): 3d bem for general anisotropic elasticity. *Int. J. Solids Struct.*, vol. 44, pp. 7073–7091.

Willis, J. (1996): Hertzian contact of anisotropic bodies. *J. Mech. Phys. Solids.*, vol. 14, pp. 163–176.

Wriggers, P. (2002): *Computational Contact Mechanics*. West Sussex, England.

Xiaoyu, J. (1995): Frictional contact analysis of composite materials. *Compos. Sci. Technol.*, vol. 54, pp. 341–348.

Zmitrowicz, A. (1989): Mathematical descriptions of anisotropic friction. *Int. J. Solids Struct.*, vol. 25, pp. 837–862.

Zmitrowicz, A. (1999): An equation of anisotropic friction with sliding path curvature effects. *Int. J. Solids Struct.*, vol. 36, pp. 2825–2848.